Accepted Article

Continental microseismic intensity delineates oceanic upwelling timing along the west coast of North America

Richard E. Thomson[1], Martin Heesemann[2], Earl E. Davis[3], and Roy A. S. Hourston[1]

[1]Fisheries and Oceans Canada, Institute of Ocean Sciences

P.O. Box 6000, 9860 West Saanich Road, Sidney, BC, V8L 4B2, Canada

[2]Ocean Networks Canada, University of Victoria

PO Box 1700 STN CSC, 2300 McKenzie Avenue Victoria, BC V8W 2Y2, Canada

[3]Pacific Geosciences Centre, Geological Survey of Canada

P.O. Box 6000, 9860 West Saanich Road, Sidney, BC, V8L 4B2, Canada

Corresponding author: Richard Thomson, Institute of Ocean Sciences, Fisheries and Oceans Canada, Sidney, British Columbia, Canada, V8L 4B2

(Richard.Thomson@dfo-mpo.gc.ca)

This article has been accepted for publication and undergone full peer review but has not been through the copyediting, typesetting, pagination and proofreading process which may lead to differences between this version and the Version of Record. Please cite this article as doi: 10.1002/2014GL061241

©2014 American Geophysical Union. All rights reserved.

Accepted Article

Abstract

The biological productivity of coastal upwelling regions undergoes marked interannual variability as marine ecosystems respond to changes in the prevailing winds. Determination of the principal metrics that define the upwelling cycle – the Spring Transition, when ocean conditions switch from downwelling- to upwelling-favorable, and the Fall Transition, when conditions return to downwelling-favorable – is essential for understanding changes in coastal productivity. Here we demonstrate that upwelling in the northern California Current System may be delineated by changes in microseismic activity recorded at a broadband seismological station in southwestern British Columbia. Observed high correlation between microseismic intensity and offshore bottom pressure fluctuations at ~0.2 Hz confirms a direct link to regional wind-wave generation. Comparison of transition times derived from coincident 20-year records of microseismic intensity and alongshore wind stress for the British Columbia-Oregon coast suggests that seismically derived times may be more representative of coastal upwelling than times derived using traditional methods.

Index terms: 4227, 4279, 4516, 4594, 4813, 7230

Key words: Microseisms; Spring and fall transitions; Coastal upwelling indices; Wind waves; California Current System; Ocean bottom pressure fluctuations

Key points:

Microseismic motions define timing of the oceanic spring and fall transitions

Microseisms are the integrated response to coastal wave-wave interactions

Twenty-year coastal upwelling records are created for California Current System

©2014 American Geophysical Union. All rights reserved.

1. Introduction

The highly productive marine ecosystems found within the eastern boundary current regions of the World Ocean are dependent on upwelling-favorable winds for the transport of primary nutrients (phosphate, silicate and nitrate) to the surface euphotic zone. On the west coast of North America, the upwelling domain extends over 3000 km from central British Columbia to the southern Baja California Peninsula (Figure 1). In the northern sector of the domain (~42-52° N latitude), the transition to spring oceanic conditions is characterized by a reversal in the prevailing winds, from strong, predominantly poleward (downwelling-favorable) in winter to moderately strong, predominantly equatorward (upwelling-favorable) in summer [*Ware and McFarlane*, 1989; *Hsieh et al.*, 1995; *Bograd et al.*, 2009]. The reverse process occurs in fall. In the southern sector, the spring transition marks a change from weak to strong equatorward winds.

The onset of sustained coastal upwelling in spring resupplies the upper ocean with nutrients and forms the basis of a bottom-up ecosystem response that supports the growth of marine organisms at all trophic levels within the upwelling system [*Ware and Thomson*, 2005]. Interannual variability in the annual upwelling cycle can affect trophic level dynamics within the coastal ocean by altering the phase relationship between phytoplankton and zooplankton growth. This can then impact the long-term productivity of higher level organisms [*Cury and Roy,* 1989; *Ware and Thomson*, 1991; *Roemmich and McGowan,* 1995; *Botsford et al*., 2006; *Ware and Thomson*, 2005; *Barth et al*., 2007]. Determining the timing of the spring and fall transitions is, therefore, important for understanding changes in the phenology and productivity of coastal marine ecosystems [*Smith*, 1978; *Smith and Eppley*, 1982; *Robinson*, 1994; *Kosro et al*., 2006; *Bograd et al*., 2009; *Thomson et al.*, 2012;

©2014 American Geophysical Union. All rights reserved.

Bylhouwer et al., 2013].

The timing of the spring and fall transitions is commonly defined in terms of the alongshore component of the wind stress. In addition to its dynamical link to upwelling processes [*Gill*, 1982; *Brink*, 1983], wind stress is also one of the more readily available environmental variables. *Bakun* [1973] used the daily-averaged alongshore wind stress derived from six-hourly geostrophic winds to produce a surrogate time series of coastal upwelling known as the Upwelling Index (*UI*). This index – in effect the cross-shore surface Ekman transport generated by the alongshore wind stress in conjunction with the Coriolis effect – has formed the backbone of most upwelling-related studies. *Strub et al.* [1987a, b] went a step further by examining the spring transition in the California Current System in terms of the prevailing wind stress, coastal sea level, alongshore currents and sea surface temperature. A recent study by *Bograd et al*. [2009] defines transition timing for the California Current ecosystem in terms of inflection points in the Cumulative (time-integrated) Upwelling Index (*CUI*).

Although the mechanistic link between coastal upwelling and wind stress is widely accepted [cf. *Bakun*, 1973; *Herman et al.*, 1989; *Schwing et al.*, 1996], wind stress is not a direct measure of the ocean's response to atmospheric forcing. Numerous steps lie between the vertical flux of momentum from the air to the ocean, the subsequent generation of a surface Ekman layer (with a cross-shore geostrophically-induced surface flow and compensating cross-shore interior flow), and the displacement of isopycnal surfaces by the vertical upwelling velocity *w* that forms at the base of the Ekman layer. This shortcoming was partially addressed by *Huyer et al*. [1979] who were among the first to include directional changes in observed alongshore currents as an indicator of the spring transition off the Oregon

Accepted Article

©2014 American Geophysical Union. All rights reserved.

coast. *Thomson and Ware* [1996] combined wind stress time series with current meter observations on the continental slope to devise a current velocity index (*CVI*) of upwelling for the coast of British Columbia. The requirement for long-term current velocity records limits application of the *CVI*.

The continuing need for indices that are representative of the integrated response of the ocean to wind forcing led us to consider surface gravity wave activity as a surrogate for coastal upwelling. Specifically, the spectra of observed wind-wave heights off the coast should be a direct measure of the spatially and temporarily integrated transfer of atmospheric momentum to the upper ocean. The annual spring-fall timing cycle can then be defined in terms of the cessation and onset of downwelling conditions associated with storm-induced wind waves. There are numerous meteorological buoys measuring waves in the coastal ocean (http://www.ndbc.noaa.gov) but these report only significant wave height and peak wave period, which may be strongly affected by distal storm events and may not, therefore, be fully representative of regional wind forcing. These limitations, together with studies showing that storm-generated waves are responsible for the relatively intense ~0.2 Hz ground motions recorded at land-based stations [e.g., *Bromirski and Duennbier*, 2002; *Kedar and Webb,* 2005; *Aster et al*., 2008; *Bromirski*, 2009; *Ardhuin et al*., 2011], suggested that we could use microseismic activity as a reliable measure of wind-generated surface wave intensity, and hence the timing of the seasonal upwelling cycle along continental margins.

In this study, we show that microseisms recorded in the 0.24±0.10 Hz (5±2 s) frequency band by seismometers located at the Pacific Geosciences Centre (PGC) on southern Vancouver Island can be used to delineate the seasonal upwelling cycle off the central Pacific coast of North America. In particular, the cessation of storm

©2014 American Geophysical Union. All rights reserved.

activity and associated downwelling along the British Columbia-Washington-Oregon coast in spring is shown to coincide with an abrupt reduction in the microseismic intensity at the PGC site that arises from surface gravity waves with periods of 10±4 s. The return to storm conditions and downwelling winds in fall coincides with an equally abrupt return to high seismic intensity. Although the connection between microseisms and wind waves has been known for over 60 years, our findings are the first to link land-based seismicity with coastal upwelling.

2. Wave-generated microseisms

In a seminal paper, *Longuet-Higgins* [1950] demonstrated that continental microseisms of around 0.2 Hz originate from bottom pressure fluctuations associated with P body waves generated through the nonlinear interaction of trains of oceanic wind waves of identical frequency, ω, traveling in opposite directions. Because the pressure fluctuations are forced by the standing wave component of the wave-wave interactions, the microseisms occur at twice the frequency of the incoming gravity waves. A subsequent analysis by *Hasselmann* [1963] showed that seafloor Rayleigh waves are generated when the vector sum, $\mathbf{K}_{12}= \mathbf{k}_1+\mathbf{k}_2$, of the nearly identical magnitude and nearly oppositely directed wavenumbers $\mathbf{k}_1$ and $\mathbf{k}_2$ of the interacting wave trains matches the wavenumber $\mathbf{K}$ of one of the possible seismic modes for given frequency ω [see also *Ardhuin and Herbers*, 2013]. This type of microseismic activity is common in coastal regions where onshore propagating trains of gravity waves are reflected from the continental boundary [*Bromirski and Duennibeir*, 2002; *Ardhuin et al.*, 2011].

Numerical simulations of wind-generated microseisms by *Ardhuin et al.*[2011, 2012] show that the wave reflection mechanism generally dominates in eastern boundary regions and is particularly dominant off central California in winter.

©2014 American Geophysical Union. All rights reserved.

Microseisms recorded at seismological stations typically represent sources within a few hundred kilometers of the coast [*Bromirski et al*., 2013]. Although microseisms generated through the interaction of two independent wind-wave systems can sometimes dominate the coastal seismological signal, such contributions are intermittent and short-lived. Strong winds can also develop along the coast in summer but are primarily alongshore. This leads to a comparatively weak cross-shore component of the directional wave spectra and to greatly reduced double-frequency microseismic noise in summer compared to winter.

3. Seismological observations

For this study, we have used the vertical ground velocity component recorded at the PGC site (Figure 1) from March 1993 to March 2013. To simplify processing, the original series sampled at 40 Hz was low-pass filtered and decimated to 1 Hz sampling. We then segmented the decimated record into block lengths of 4096 s with offsets of 900 s (15 min) between adjoining segments. Times were chosen such that the first 15-min record is centered at 00:00 UTC on January 1, 1993. Prior to spectral analysis, each segment was linearly detrended and smoothed using a Hanning window with a half width of 2048 s [cf. *Thomson and Emery*, 2014]. We then used a Fast Fourier Transform (FFT) to derive the spectral power density, $S_k(\omega)$, for each 15-min segment (k = 1, 2, ..., N; $N = 7\times10^5$). If a given segment had data gaps, the power spectrum for that segment was classified as missing (NAN). Each spectral estimate extends from the Nyquist frequency (0.5 Hz) to the segment sampling frequency (2.44×10^{-4} Hz), corresponding to periods of 2 to 4096 s. Each windowed spectral estimate has roughly 1.6×2 degrees of freedom.

As illustrated by Figure 2a, the spectral density of the high-frequency microseismic signal (periods < 10 s) greatly exceeds that of the low-frequency signal

©2014 American Geophysical Union. All rights reserved.

arising from long period swell and infragravity waves (periods > 40 s; often referred to as the Earth's "hum"; *Webb*, 2007). The seismic record also shows a marked spectral roll-off for periods less than 3 s. Visual comparison of Figure 2a with Figure 2b reveals that the high frequency seismic signal variations have a near one-to-one correspondence with variations in high frequency bottom pressure recorded at Ocean Drilling Program (ODP) CORK site 1026 located in 2660 m of water off the west coast of Vancouver Island (Figure 1). In contrast, the relatively intense bottom pressure variations in the infragravity wave band in Figure 2b are not present in Figure 2a. The strong similarity between the high frequency components of the two data records, supported by similar results we have derived for nearby bottom pressure sensors at Ocean Networks Canada cabled observatory locations in Barkley Canyon and slope site 889, confirms that the microseismic signals are generated quite locally by wave-induced bottom pressure fluctuations.

Because our focus is on microseismic activity, we truncated the ends of the 15-min seismic spectra at periods of 3 and 7 s and then calculated the integrated spectral density, $\overline{S}_k$, over the range of 3 to 7 s. Spectra at periods longer than 7 s typically display sloping (i.e., time varying) distributions characteristic of highly dispersive swell with periods longer than 14 s arriving on the west coast from as far away as the Southern Ocean, which are not representative of regionally forced wind waves. Spectra with periods less than 3 s are associated with wind waves with periods less than 6 s, which contribute little to the integrated spectra. Thus, integrated spectra are primarily determined by vertical ground motions with periods of 5±2 s.

Short-duration seismic wave trains from earthquakes are evident throughout the 15-min spectra (Figure 2a) and can lead to anomalously high spectral values. Rather than removing individual earthquake events, we eliminated their effect by

©2014 American Geophysical Union. All rights reserved.

Accepted Article

calculating the median value, $\overline{S}_j^m$, for running 6-hr segments of the band-integrated seismic spectra (j = 1, 2, ..., M; $M << N$). Six-hourly data segments with fewer than 16 spectral values were designated as missing. Of the roughly three-quarters of a million six-hourly values in the 20-year PGC record, only 9.8% were designated as missing. For periods less than 10 s, the median spectral time series of the PGC record closely resembles that for the CORK pressure record (Figure S1), thus confirming the strong link to high frequency bottom pressure variations.

4. Determination of the spring and fall transitions

To compare our seismologically derived results with traditional wind-derived upwelling indices, we have used the cumulative upwelling index (*CUI*) approach of *Bograd et al*. [2009]. The method is based on time series of the mean upwelling index, *UI*, which is equivalent (except in equatorial regions) to the alongshore component of wind stress, τ_y, through the relationship, $UI = -\tau_y/(\rho f)$; ρ is the water density and f is the local Coriolis parameter. Because τ_y is positive in the poleward direction, upwelling occurs during times of negative (equatorward directed) wind stress. An advantage of the cumulative upwelling index, $CUI_J = \sum_{j=1}^{J} UI_j$, and the slightly modified version

$$CUI_{\tau,J} = \sum_{j=1}^{J} \tau_{y,j} = -\rho f CUI_J \qquad (3)$$

used in this study, is that it does not require event-detection algorithms to pick out the transition dates in the time series. Specifically, CUI_τ defines the spring transition as the Julian day, J, from the beginning of the calendar year when the cumulative upwelling reaches its maximum value (j = 1 corresponds to 0300 UTC on 1 January); here, upwelling is negative and downwelling is positive. Similarly, the fall transition

©2014 American Geophysical Union. All rights reserved.

Accepted Article

corresponds to the day when the cumulative upwelling reaches its minimum value. Note that because we use wind stress directly, the sign of CUI_τ is consistent with the results to be derived from the seismic data but is the reverse of *CUI* used by *Bograd et al*. [2009].

The variable CUI_τ has been calculated using the gridded (1.9° latitude × 1.9° longitude) wind stress (momentum flux) data from the NCEP/NCAR Reanalysis-1 data set [*Kalnay et al*., 1996; *Kistler et al*., 2001], which is coarser than the 1° × 1° grid resolution of the U.S. Navy Fleet Numerical Meteorological and Oceanography Center (FNMOC) data used by *Bograd et al*. [2009]. As with *Bograd et al*. [2009], we use 6-hourly values in order to capture as much of the available wind stress variability as possible. Time series of CUI_τ for Reanalysis-1 sites off southwest British Columbia, central Washington and northern Oregon for 2012 are presented in Figure 3a. As was the case for 2012, the spring and fall transition dates for the three wind sites (Figure 1) typically differ by only a few days. However, as Figure 3a also illustrates, this difference can jump by several weeks if the cumulative sums have a broad flat peak; differences in peak values may be small but there can be major differences in their respective timing dates. There is no formal methodology for providing confidence estimates for timing dates derived from the wind stress or *UI* records.

Prior to generating a cumulative upwelling index from the microseismic record, we first replaced zeroes in the 6-hourly microseismic spectral time series, $\overline{S}_j^m$, with NAN (missing) and then transformed the series to $\log\left(\overline{S}_j^m\right)$. In addition to enabling us to use standard statistical methods, the log-transform has a physical justification in that the energy of the wind waves generating the microseisms has a

©2014 American Geophysical Union. All rights reserved.

power-law dependence on wind duration, speed and fetch [*Komen et al*., 1994; *Ardhuin et al.*, 2011]. To more closely emulate the positive and negative phases of the upwelling index (*UI*), we next generated 6-hourly residual time series $\log\left(\overline{S}_j^m\right)^* = \log\left(\overline{S}_j^m\right) - \overline{\log\left(\overline{S}_j^m\right)}$ by subtracting a year-specific mean, $\overline{\log\left(\overline{S}_j^m\right)}$ (defined in the next section), from the spectrally integrated seismic record for each year. The calculation of residual time series should also prove useful when applying the cumulative sum method to regions, such as southeast Alaska, that lack distinct seasonally reversing prevailing wind directions. In this case, the transitions would demark changes between strong and weak downwelling periods.

We have determined the seismic cumulative upwelling index,

$$CUI_{S,J} = \sum_{j=1}^{J} \log(\overline{S}_j^m)^* \qquad (4)$$

for the PGC site for 1993 to 2013 by integrating the 6-hourly residual seismic record $\log\left(\overline{S}_j^m\right)^* \equiv \overline{S}^m(t)$ starting at time t = 00 hours on 1 January of each year. Of the various possible choices for averaging periods for the log-transformed seismic records, we confined our analysis to those for 1 January-31 May, 1 January-30 June, and 1 January-31 July since they bracket the period when the spring transition is most likely to occur in the region. Figure 3b presents the CUI_S for the three averaging periods for 2012. Except for 1998, which has missing seismic data in early February and for which the spring transition date is ambiguous regardless of averaging period (Figure S2), the January-June averaging period yielded spring and fall transition times that agreed most closely with those based on visual inspection of all years and was selected to define the nominal seismic transition dates and other seasonal parameters. Transition dates for averaging periods January-May and January-July straddle those

©2014 American Geophysical Union. All rights reserved.

Accepted Article

for the January-June period and can be used to gauge the uncertainty in the seismically determined transition dates. Support for this approach is derived from the fact that the spring transition dates based on the January-June period agree with one or both of the dates obtained using the January-May and January-July averaging periods. Similar results are obtained for the fall transition dates. (For 1998, the Spring Transition date is based on the January-May averaging period since it has the least ambiguous CUI_S distribution.)

5. Results and Discussion

As illustrated by Figure 4a, the 20-year time series of the spring transition calculated using CUI_S for the PGC seismological site differs from the corresponding CUI_τ series obtained for the alongshore wind stress for the Reanalysis-1 sites off British Columbia, Washington and Oregon. The greatest difference is the exaggerated interannual variability in the wind-derived spring transition series compared to the seismically derived series. As in 2001 and 2005, the wind records sometimes yield highly anomalous spring transition times relative to the long-term mean, which does not occur in the seismic data. Differences in the spring transitions derived from the two types of data are as large as 50 days, and differences of 30-40 days are not uncommon. This contrasts with typical differences of only days among the three transition series derived using the Reanalysis winds (Table S1). In addition to the yearly differences, findings show that the mean wind-derived spring transition dates for southern British Columbia, central Washington and northern Oregon (mean ± standard deviation of 4 April±27 d, 6 April±26 d, and 7 April±29 d, respectively) are earlier than the mean seismically derived date of 10 April±17 d and have twice the standard deviation. The seismically-defined spring transition series also has a negative trend from 1993 to 2002, which is not present in the wind-derived series.

©2014 American Geophysical Union. All rights reserved.

As with the spring transition, the wind-derived fall transition series are similar for the British Columbia, Washington and Oregon coasts but have much greater interannual variability than the seismically derived fall series (Figure 4b; Table S1). Again, differences in the fall transition times between the two types of data can differ by as much as 50 days. The mean fall transition times derived from the wind data for the British Columbia, Washington and Oregon sites (17 October±20 d, 16 October±17 d, and 20 October±20 d, respectively) are considerably later than the seismically derived date of 7 October±11 d (JD 280±11 d) and have twice the standard deviation. Similar differences are found between the wind-derived and seismically derived summer duration time series obtained by subtracting the fall and spring transition dates (Figure 4c). The mean summer duration for the seismic record (180±22 d) is markedly shorter than the summer duration for the wind stress records (~195±30 d).

One reason for the differences between the two methods is that the wind-derived spring transition date is sometimes determined by a short burst of upwelling-favorable winds in late winter or early spring that follow a sustained period of downwelling. Such events can occur during strong outflow wind conditions that accompany the formation of high pressure over the Arctic in winter. Even though conditions return to a protracted period of strong downwelling-favorable winds within a few days (as in early February 2001), the wind-based CUI_{τ} algorithm picks the early peak value as a very early "false spring" transition. Similarly, a sudden downwelling event a month or so after the apparent end of winter can cause the CUI_{τ} to remain high, leading to a peak in late spring, as in May 2005.

In summary, microseismic records of vertical ground velocity from land-based seismological stations can be used to delineate the spring and fall transitions in the northern California Current upwelling system where microseisms are dominated by

Accepted Article

©2014 American Geophysical Union. All rights reserved.

the double frequency wave reflection generation mechanism in winter (*Ardhuin et al*., 2011, 2012). By extension, it might be possible to use the global network of seismic stations to examine biologically relevant processes in coastal regions of the World Ocean. While we favor the seismically determined transition times over the wind-derived times, just which sets of transition dates most closely relate to interannual variations in coastal primary production remains an open question that we leave to a more detailed follow-on study.

Acknowledgements

We thank staff at the Pacific Geosciences Centre for providing us the seismic record and Patricia Kimber for drafting the figures. The manuscript also benefited from two very helpful anonymous reviews. NCEP Reanalysis data are from the NOAA/OAR/ESRL PSD Website http://www.esrl.noaa.gov/psd/.

References

Ardhuin, F., E. Stutzmann, M. Schimmel, and A. Mangency (2011), Ocean wave sources of seismic noise, *J. Geophys. Res.,116*, C09004, doi:10.1029/2011JC006952.

Ardhuin, F., A. Balanche, E. Stutzmann, and M. Obrebski (2012), From seismic noise to ocean wave parameters: General methods and validation, *J. Geophys. Res.,117*, C05002, doi:10.1029/2011JC007449.

Ardhuin, F., and T. H. C. Herbers (2013), Noise generation in the solid Earth, oceans and atmosphere, from nonlinear interacting surface gravity waves in finite depth, *J. Fluid Mech.*, *716*, 316-348.

Aster, R. C., D. E. McNamar, and P. D. Bromirski (2008), Multidecadal climate-induced variability in microseisms, *Seismological Res. Lett.,*79(2), doi:10.1785/gssrl.79.2.194.

Bakun, A. (1973), Coastal upwelling indices, west coast of North America, 1946-71,

©2014 American Geophysical Union. All rights reserved.

Tech. Rep. NMFS SSRF-671, pp. 103, Natl. Oceanic and Atmos. Admin., Seattle, Washington.

Barth, J. A., B. A. Menge, J. Lubchenco, F. Chan, J. M. Bane, A. R. Kirincich, M. A. McManus, K. J. Nielsen, S. D. Pierce, and L. Washburn (2007), Delayed upwelling alters nearshore coastal ocean ecosystems in the Northern California Current, *PNAS, 104*(10), 3719-3724, doi:10.1073/pnas.0700462104.

Bograd, S. J., I. Schroeder, N. Sarkar, X. Qiu,W. J. Sydeman, and F. B. Schwing (2009), Phenology of coastal upwelling in the California Current, *Geophys. Res., Lett., 36*, L01602, doi:10.1029/2008GL035933.

Botsford, L.W., C. A. Lawrence, E. P. Dever, A. Hastings, and J. Largier (2006), Effects of variable winds on biological productivity on continental shelves in coastal upwelling systems, *Deep-Sea Research II, 53*, 3116–3140.

Brink, K. H. (1983), The near-surface dynamics of coastal upwelling, *Prog. Oceanogr. 12*, 223-257.

Bromirski, P. D. (2009), Earth vibrations, *Science*, *324*, 1026-1027.

Bromirski, P. D. and F.K. Duennebeir (2002), The near-coastal microseism spectrum: Spatial and temporal wave climate relationships, *J. Geophys. Res.*, *107*, NO. B8, 10.1029/2001JB000265.

Bromirski, P. D., R. A. Stephen, and P. Gerstoft (2013), Are deep-ocean-generated surface-wave microseisms observed on land?, *J. Geophys. Res.*, *118*, 1-20, 10.1002/jgrb.50268.

Bylhouwer, B., D. Ianson, and K. Kohfeld (2013), Changes in the onset and intensity of wind-driven upwelling and downwelling along the North American Pacific coast, *J. Geophys. Res. Oceans*, *118*, 2565–2580, doi:10.1002/jgrc.20194.

Cury, P., and C. Roy (1989), Optimal environmental window and pelagic fish

Accepted Article

©2014 American Geophysical Union. All rights reserved.

Accepted Article

recruitment success in upwelling areas, *Can. J. Fish. Aquat. Sci.*, *46*, 670-680.

Gill, A. E. (1982), *Atmosphere-Ocean Dynamics*, pp. 662, Academic Press, San Diego, Calif.

Hasselmann, K. (1963), A statistical analysis of the generation of microseisms, *Reviews of Geophysics*, *1*, 177–210.

Hermann, A. J., B. M. Hickey, M. R. Landry, and D. F. Winter (1989), Coastal upwelling dynamics, in *Coastal Oceanography of Washington and Oregon*, Editors M. R. Landry and B. M. Hickey, pp. 211-253, Elsevier, Amsterdam.

Hsieh, W. W., D. M. Ware, and R. E. Thomson (1995), Wind-induced upwelling along the west coast of North America, 1899-1988, *Can. J. Fish. Aquat. Sci.*, *52*, 325-334.

Huyer, A., E. J. Sobey and R. L. Smith (1979), The spring transition in currents over the Oregon continental shelf, *J. Geophys. Res.*, *84*, 6995-7011.

Kalnay, E., M. Kanamitsu, R. Kistler, W. Collins, D. Deaven, L. Gandin, and D. Joseph, (1996), The NCEP/NCAR 40-year reanalysis project. *Bulletin of the American meteorological Society*, *77*(3), 437-471.

Kedar, S., and F. H. Webb (2005), The ocean's seismic hum, *Science*, *307*, 682.

Kistler, R., and Coauthors (2001), The NCEP–NCAR 50-Year Reanalysis: Monthly means CD-ROM and documentation. *Bull. Amer. Meteor. Soc.*, *82*, 247–268.

Komen, G. J., L. Cavaleri, M. Donelan, K. Hasselmann, S. Hasselmann and P. A. E. M. Janssen (1994), *Dynamics and Modelling of Ocean Waves*, pp. 532, Cambridge University Press.

Kosro, P. M, W. T. Peterson, B. M Hickey, R. K. Shearman, S. D. Pierce (2006), The physical vs. the biological spring transition: 2005, *Geophys. Res. Lett*, *33* (22), (L22S03), doi:10.1029/2006GL02707.

Longuet-Higgins, M. S. (1950), A theory of the origin of microseisms, pp. 35,

©2014 American Geophysical Union. All rights reserved.

Philosophical Transactions of the Royal Society of London. Series A, Mathematical and Physical Sciences, *243*.

Roemmich, D., and J. McGowan (1995), Climatic warming and the decline of zooplankton in the California Current, *Science*, *267*, 1324-1326.

Robinson, C. L. K. (1994), The influence of ocean climate on coastal plankton and fish production, *Fish. Oceanogr.*, *3*, 159-171.

Schwing, F. B., M. O'Farrell, J. M. Steger, and K. Baltz (1996), Coastal upwelling indices, West Coast of North America, 1946 – 1995, pp. 104, NOAA Tech. Memo., NOAA-TM-NMFS-SWFSC-231.

Smith, P. E. (1978), Biological effects of ocean variability: time and space scales of biological réponse, *Rapp. P.-v. Réun. Cons. int. Explor. Mer*, *173*, 117-127, 1978.

Smith, P. E., and R. W. Eppley (1982), Primary production and the anchovy population in the southern California bight: comparison of time series, *Limnol. Oceanogr.*, *27*, 1-17.

Strub, P. T., J. S. Allen, A. Huyer, R. L. Smith, and R. C. Beardsley (1987a), Seasonal cycles of currents, temperatures, winds, and sea level over the northeast Pacific continental shelf: 35°N to 48°N, *J. Geophys. Res.*, *92,* 1507-1526.

Strub, P. T., J. S. Allen, A. Huyer, and R. L. Smith (1987b), Large-scale structure of the spring transition in the coastal ocean off western North America, *J. Geophys. Res.*, *92*, 1527-1544.

Thomson, R. E., and D. M. Ware (1996), A current velocity index of ocean variability. *J. Geophys. Res.*, *101*, 14,297-14,310.

Thomson, R. E., R. J. Beamish, T. D. Beacham, M. Trudel, P. H. Whitfield and R. A. S.

Hourston (2012), Anomalous ocean conditions may explain the recent extreme

Accepted Article

©2014 American Geophysical Union. All rights reserved.

Accepted Article

variability in Fraser River sockeye salmon production, *Marine and Coastal Fisheries: Dynamics, Management, and Ecosystem Science*, *4*(1), 415-437, doi.org/10.1080/19425120.2012.67598.

Thomson, R. E., and W. J. Emery (2014), *Data Analysis Methods in Physical Oceanography*, 3rd edition, pp. 750, Elsevier Science.

Ware, D. M., and G. A. McFarlane (1989), Fisheries production domains in the northeast Pacific Ocean, in *Effects of Ocean Variability on Recruitment and an Evaluation of Parameters used in Stock Assessment Models*, Editors R. J. Beamish and G. A. McFarlane, *Can. Spec. Publ. Fish. Aquat. Sci.*, *108*, 359-379.

Ware, D. M., and R. E. Thomson (1991), Link between long-term variability in upwelling and fish production in the northeast Pacific Ocean, *Can. J. Fish. Aquat. Sci.*, *48*, 2296-2306.

Ware, D. M. and R. E. Thomson (2005), Bottom-up ecosystem trophic dynamics determine fish production in the northeast Pacific, *Science*, *308*, 1280-1284.

Webb, S. C. (2007), The Earth's 'hum' is driven by ocean waves over the continental shelves, *Nature*, *445*, doi:10.1038/nature05536.

©2014 American Geophysical Union. All rights reserved.

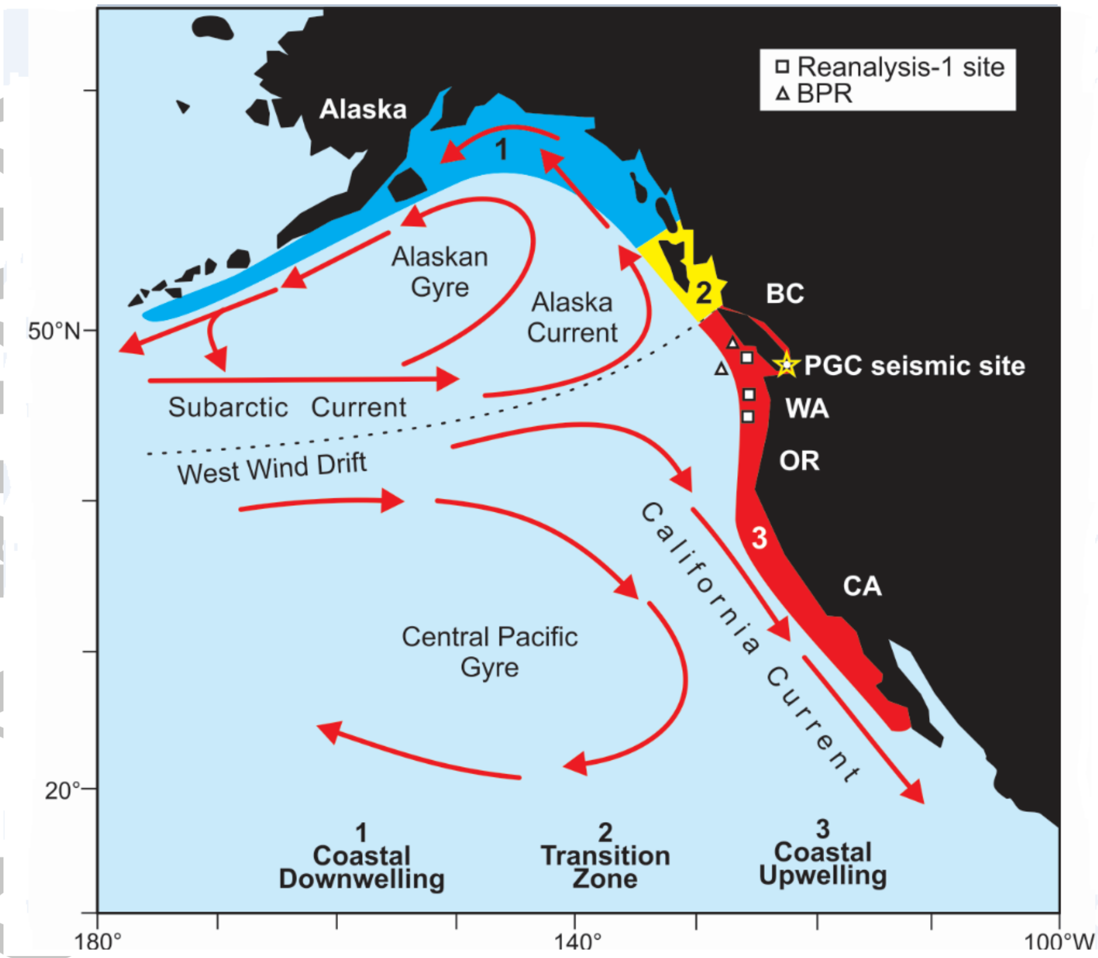

Figure 1. Upwelling domains and prevailing currents off the west coast of North America. Also shown are locations of the PGC seismic station (star at 48° 39’ N; 123° 27’ W), the three NCEP/NCAR Reanalysis-1grid points off the British Columbia, Washington and Oregon coasts (open squares at 48° 34.2’ N, 125° 37.5’ W; 46° 40.0’ N 125° 37.5’ W; and 44° 45.7’ N, 125° 37.5’ W, respectively) and the bottom pressure recorders (triangles) at ODP borehole CORK 1026 (47° 45.8’ N, 127° 45.6’ W) and Ocean Networks Canada (ONC) location 889 (48° 40.2’ N, 126° 50.9’ W). The Barkley Canyon bottom pressure recorder is near the northern Reanalysis site.

©2014 American Geophysical Union. All rights reserved.

Accepted Article

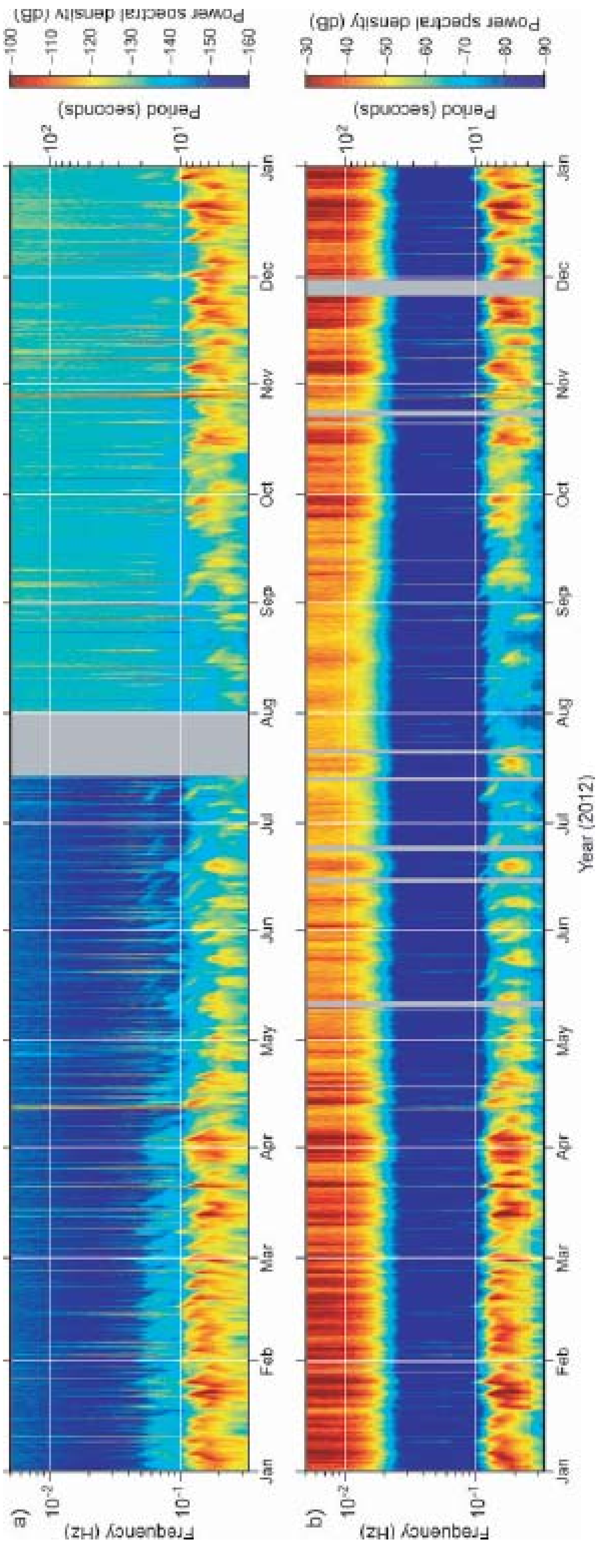

Figure 2. Time series of 15-min spectral estimates derived using 1 Hz seismic vertical velocity and ocean bottom pressure records for the west coast of Canada during 2012. (a) Spectral density, $S_k(\omega)$, in $(m/s)^2$/Hz for the seismic record from the PGC seismological station and (b) same as (a) but in $(dbar)^2$/Hz for the bottom pressure

©2014 American Geophysical Union. All rights reserved.

spectra from 2660 m depth at CORK site 1026 in Cascadia Basin (1 dbar = 10^4 Pa). Gray segments denote gaps in the original data or times of anomalously low spectral values. The gap in the seismic record during February 1998 was due to instrument failure while that in July 2012 was the result of a lightning strike. The gap in 1998 was filled using linear regression of the microseismic record against the significant wave height measured at meteorological buoy MB46206 off southwest Vancouver Island (48° 34.2' N, 125° 37.5' W) for the two weeks preceding the gap (Figure S2); the 2012 gap was left unfilled as it did not affect transition times.

Accepted Article

©2014 American Geophysical Union. All rights reserved.

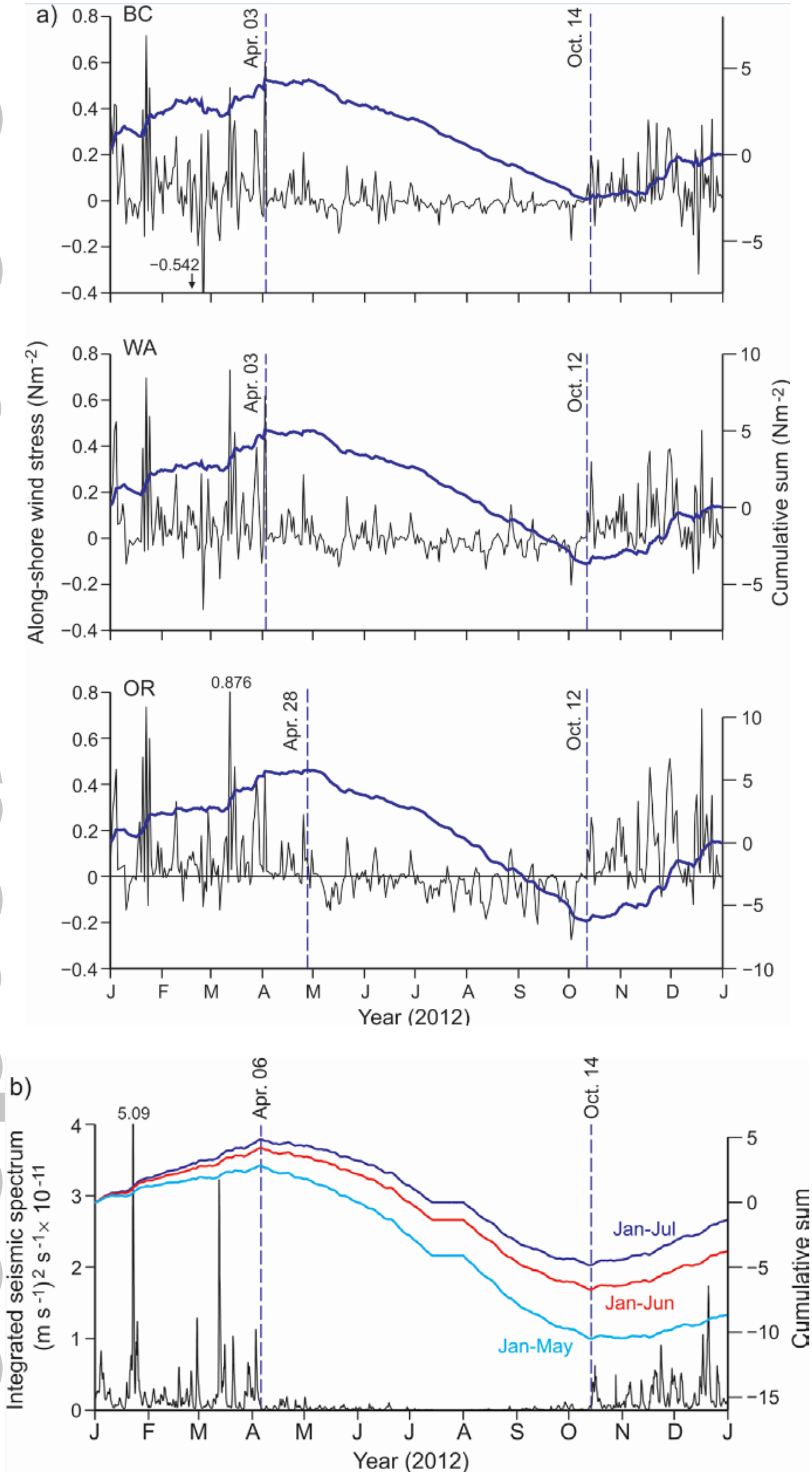

Figure 3. Time series of input data (thin lines) and resulting cumulative upwelling indices (thick lines) for southern British Columbia and the Pacific Northwest of the

Accepted Article

©2014 American Geophysical Union. All rights reserved.

United States for 2012. Vertical lines give the derived dates of the spring and fall transitions. Peak input values outside the plotting range have been labelled. (a) Cumulative upwelling index, CUI_τ , based on six-hourly alongshore wind stress for the three Reanalysis-1sites (Figure 1); and (b) Cumulative upwelling index, CUI_S, calculated using the six-hourly spectra of vertical ground velocity at the PGC site. CUI_S values for the averaging period January-June (in bold) are considered most representative of the annual upwelling cycle for the study region.

Accepted Article

©2014 American Geophysical Union. All rights reserved.

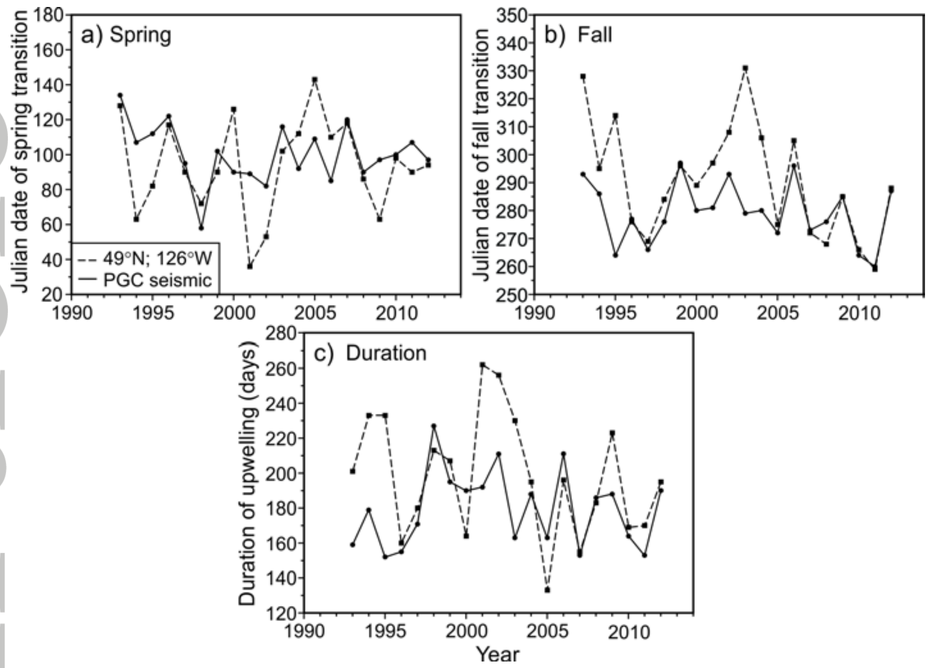

Figure 4. Time series of transition dates in Julian days derived from the alongshore component of wind stress off southwestern British Columbia and from the integrated seismic ground motion spectra for the PGC site. Julian day 1 corresponds to January 1. (a) Spring transition; (b) Fall transition; and (c) summer duration. Seismically-derived values (solid lines) in each panel are for the nominal January-June averaging period.

Accepted Article

©2014 American Geophysical Union. All rights reserved.